Matching Layers in Bragg Reflection Waveguides for Enhanced Nonlinear Interaction

Payam Abolghasem, *Student Member, IEEE*, and Amr S. Helmy, *Senior Member, IEEE*

***Abstract*—Bragg reflection waveguides (BRWs) with matching layers placed between the core and claddings are proposed and analyzed as a means of enhancing the effective second-order optical nonlinearity. The addition of matching layers to conventional BRW structures provides extra degrees of freedom, which enable further optimization to enhance the nonlinear conversion efficiency. Pertinent parameters including overlap between modal profiles of the interacting waves, the group velocity mismatch and group velocity dispersion are examined. The structures studied in this work are designed using the GaAs–$Al_xGa_{1-x}As$ material system. It is shown that, in comparison to phase-matched BRWs with no matching layers, the proposed structure benefits from relaxing the constraint over the phase-matched core thickness. For typical designs, it is shown that the new structure can provide over an order of magnitude enhancement in nonlinear coupling efficiency and 30% decrease in group velocity mismatch. It is also shown that the group velocity dispersion of the first and second harmonics are reduced by 10% and 52%, respectively.**

***Index Terms*—Bragg reflection waveguides (BRWs), nonlinear optics, optical nonlinearities in semiconductors, phase matching, second-harmonic generation, second-order nonlinearities.**

I. Introduction

HARNESSING effective ultrafast nonlinear (NL) interactions in active optoelectronic structures has received increased attention in recent years, in particular, second-order nonlinearities that enable frequency-mixing operations. Frequency mixing can be advantageous to numerous fields including applications in optical networks, sensing, and biomedical diagnostics. Despite having large nonlinear coefficients, semiconductors prove to be difficult to use as nonlinear materials due to their dispersive properties near the bandgap, where nonlinearities are maximized. This dispersive behavior renders the process of phase matching (PM), which is essential for efficient utilization of second-order nonlinearities, particularly challenging. Many techniques have been devised to achieve PM in semiconductors such as quasi-phase matching [1], form birefringence [2] and high-Q resonant cavities [3]. Recently, Bragg reflection waveguides (BRWs) have been proposed as an attractive method to achieve PM in active, monolithic platforms, where optoelectronic devices are realized [4]–[6]. The technique has the advantage of providing low-loss propagation for the interacting modes while being amenable to monolithic integration with conventional optoelectronic devices. These benefits provide clear advantages over some of the existing techniques discussed in [1]–[3]. While progress is being made in optimizing BRWs to enhance their utilization of the large $\chi^{(2)}$ nonlinearities available in $Al_xGa_{1-x}As$ [7], [8], the method could be further improved through introducing additional design parameters within the structures. More efficient nonlinear interaction and more versatile device functionality can be achieved when a larger number of tunable design parameters is available. This would enable PM with simultaneous tuning of various linear/nonlinear properties of the interacting waves. In conventional BRWs, clear tradeoffs exist between the design parameters which limits the attainable effective nonlinearities in SHG devices.

In this study, we introduce an extra degree of freedom for optimizing BRWs through utilizing matching layers between the core and both transverse Bragg reflectors (TBRs). This technique was initially introduced by Mizrahi *et al.* [9] to control the field profile and dispersion properties of air core planar and cylindrical BRWs for use in particle accelerators [10] and high power lasers. The addition of matching layers is an attractive route because it enhances the flexibility in device optimization without compromising the ease of design gained while operating at the quarter-wave point (QtW) of the TBR reflection spectrum [5]. Operating at the QtW point provides analytical, closed-form formulas for the device parameters, which affords greater insight into device optimization. While an optimization of the Bragg stack deviating from the QtW point can be undertaken to design a BRW with a given performance, this is often carried out numerically, with much reduced insight into device design. The process of second-harmonic generation (SHG) of a pump at 1550 nm will be used as a metric to assess the improvements provided by the matching layers to BRWs [7]. However, the results are generic and apply to other parametric processes. For efficient conversion of the pump, the effective usable $\chi^{(2)}$ should be maximized. This can be carried out through maximizing the overlap integral between the fundamental (FH) and the second harmonic (SH) in the waveguide core [5]. In addition, reducing the propagation losses can also enhance the conversion efficiency. Another means of enhancing the efficiency of the nonlinear interaction would be to enhance the effective interaction length between the FH and SH. This can be achieved by slowing the wave propagation in the waveguide [11]. Reducing the group velocity mismatch (GVM) between the FH and SH also serves the same purpose. In device applications where short pulses propagate in the structures, group velocity

Manuscript received July 31, 2008; revised September 14, 2008. Current version published May 13, 2009. This work was supported by the Natural Sciences and Engineering Research Council of Canada (NSERC) Discovery grant 293258/5 and by Champions of Innovations grants from Ontario Centers of Excellence.

The authors are with the Edward S. Rogers Sr. Department of Electrical and Computer Engineering and the Institute of Optical Sciences, University of Toronto, Toronto, ON M5S 3G4, Canada (e-mail: payam.abolghasem@utoronto.ca; a.helmy@utoronto.ca).

Digital Object Identifier 10.1109/JQE.2009.2013118

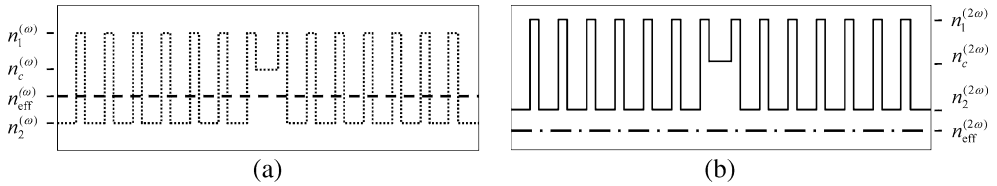

Fig. 1. Index profile of a sample BRW. (a) The dotted line shows the profile of the layers at ω where the dashed line indicates the effective index of the TIR mode. (b) Index profile at 2ω where the solid line shows the profile of the layers and the dashed–dotted line indicates the effective index of the Bragg mode. Both effective indexes at ω and 2ω have strong dependence on the core dimension. For PM SHG, the core thickness is designed such that it aligns the two effective indexes such that $n_{\text{eff}}^{(2\omega)} = n_{\text{eff}}^{(\omega)}$.

dispersion (GVD) is an important parameter to control because it governs the pulse shape evolution with propagation and hence will influence the attainable peak power. As such, the aforementioned parameters will be discussed here and the improvements afforded by using matching layer-based BRWs will be compared and contrasted with those achievable using conventional BRWs.

This paper is organized as follows. Section II briefly reviews PM using BRWs and highlights its major limitations. In Section III, the modal dispersion relations and design equations of BRWs with matching layers are presented. Section IV provides the simulation results, where representative BRWs with matching layers were analysed. Conclusions are then given in Section V.

II. Tradeoffs and Limitations in PM Using BRWs

BRWs aide modal PM between the harmonics through their versatile modal dispersion properties. In this scheme, the FH (ω) propagates as a total internal reflection (TIR) mode with an effective index, $n_{\text{eff}}^{(\omega)}$, which satisfies the condition

$$n_{\min}^{(\omega)} < n_{\text{eff}}^{(\omega)} < n_c^{(\omega)} \tag{1}$$

where $n_c^{(\omega)}$ is the core index and $n_{\min}^{(\omega)}$ is the minimum refractive index between cover and substrate at ω. The SH (2ω) with an effective index $n_{\text{eff}}^{(2\omega)}$ propagates as a Bragg mode. The Bragg modes indexes are bounded by the material indexes to ensure nonevanescent field throughout the structure, which translates to the leaky condition

$$0 < n_{\text{eff}}^{(2\omega)} < n_{\min}^{(2\omega)}. \tag{2}$$

Here, $n_{\min}^{(2\omega)}$ is the minimum material index between the cover and substrate at 2ω. The refractive index profiles of the FH and the SH with their associated effective indexes for an unphase-matched structure are plotted in Fig. 1, where n_1 and n_2 are the indexes of the TBRs layers. The substrate and cover are both taken as n_2. The strong modal dispersion properties of the Bragg modes can be employed to align the mode indexes of the FH and SH. This technique was introduced in [4] and was successfully demonstrated in [7] and [8]. The first demonstration was for Type-I PM, where the TE-polarized TIR-guided FH was phase-matched to a TM-polarizated Bragg mode-guided SH. The PM condition can be expressed as

$$n_{\text{eff}}^{\text{TE}(\omega)} = n_{\text{eff}}^{\text{TM}(2\omega)}. \tag{3}$$

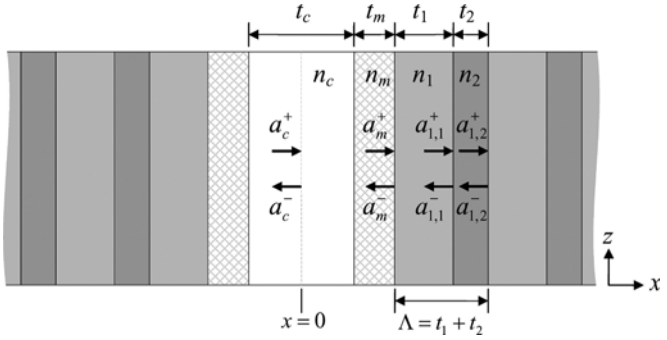

Fig. 2. Schematic of a BRW with a matching layer with refractive index n_m and thickness t_m. The structure is symmetric with respect to the core center at $x = 0$.

To maximize the conversion efficiency, multidimensional optimization methods are required. The parameter space spanned is determined by practical epitaxial growth limitations and the refractive index range available within the material system used. This governs the ultimate conversion efficiency attainable using a given material system. Operating at the QtW point introduces limitations and hence tradeoffs. One such limitation exists in the constraint imposed by the PM condition over the core thickness. Also, low loss propagation is obtained at the expense of reducing the overlap integral between the FH and SH. Another constraint is related to the periodic cladding; the choice of cladding indexes which maximize the overlap integral and hence the conversion efficiency often corresponds to regimes with high GVM between the harmonics [20]. This drastically reduces the useful device length [21]. Optimization methods based on evolutionary algorithms seem like a strong candidate for the design of these structures. However, the advantage of having the insight of designing the device using analytical closed-form expressions is often lost when using such numerical techniques.

III. Mode Equations of BRWs With Matching Layers Included

A typical symmetric BRW with a matching layer (BRW-ML) is illustrated in Fig. 2. The claddings periodicity extends in the x-direction, while the structure is homogeneous in the yz-plane. By convention, the TBRs consist of bi-layers with refractive indexes n_1 and n_2 with associated thicknesses t_1 and t_2 and periodicity $\Lambda = t_1 + t_2$. The choice and arrangement of n_1 and n_2 is further explained in Section IV. The core has an index of refraction n_c and thickness t_c. The matching layer is located between the core and quarter-wave TBRs. The refractive index of

the matching layer is n_m and the layer thickness is t_m. Mizrahi *et al.* have investigated the properties of these structures for controlling the phase velocity of Bragg modes as well as the field and power distribution within air core planar and cylindrical waveguides [9]. Their analysis was based on applying appropriate boundary conditions for field transition between the matching layer and the first Bragg reflector layer for the case that $n_m = n_2$. In this study, Bloch–Floquet formalism is employed to extend this idea to nonair-core waveguides with arbitrary n_m.

For a plane wave propagating along the $+z$-direction, the general solution of the wave equation takes the form of

$$\psi(x,y,z,t) = \psi(x)e^{i(\omega t - \beta z)} \tag{4}$$

where $\beta = k_0 n_{\text{eff}}$ is the propagation constant, k_0 is the wavenumber in free space, n_{eff} is the effective mode index, and $\psi(x)$ is the field envelope in the transverse direction, along the x-axis which satisfies the Helmholtz equation

$$\frac{d^2\psi(x)}{dx^2} + k_0^2\left[n^2(x) - n_{\text{eff}}^2\right]\psi(x) = 0. \tag{5}$$

For TE-polarized propagation with nonzero field components (H_x, E_y, H_z), $\psi(x) = E_y$ while for TM-polarization with field components (E_x, H_y, E_z), $\psi(x) = H_y$. In (5), $n(x)$ is the refractive index of the medium, which is a piecewise continuous function of x and is periodic in the claddings with a period Λ, such that $n(x+\Lambda) = n(x)$. The field distribution inside the core, matching layer and the Bragg stacks can be expressed as

$$\psi_j(x) = \begin{cases} a_c^+ e^{-ik_c x} + a_c^- e^{ik_c x} \\ 0 \le x \le t_c/2 \\ a_m^+ e^{-ik_m(x-\Delta_m)} + a_m^- e^{ik_m(x-\Delta_m)} \\ t_c/2 \le x \le \Delta_m \\ a_{j,1}^+ e^{-ik_1(x-\Delta_j+t_2)} + a_{j,1}^- e^{+ik_1(x-\Delta_j+t_2)} \\ (j-1)\Lambda + \Delta_m \le x \le j\Lambda + \Delta_m - t_2 \\ a_{j,2}^+ e^{-ik_2(x-\Delta_j)} + a_{j,2}^- e^{+ik_2(x-\Delta_j)} \\ j\Lambda + \Delta_m - t_2 \le x \le j\Lambda + \Delta_m \end{cases} \tag{6}$$

where $\Delta_m = t_c/2 + t_m$, $\Delta_j = \Delta_m + j\Lambda$ $(j = 1, 2, \ldots)$, the terms $a_{j,1}^+$ and $a_{j,1}^-$ are the field amplitudes of the right and left traveling waves in the layer with refractive index n_1 of the jth unit cell of TBRs, respectively, and $a_{j,2}^+$ and $a_{j,2}^-$ are those in the layer with refractive index n_2. The field amplitudes within the core are a_c^+ and a_c^-, and those within the matching layer are a_m^+ and a_m^-. Also in (6), k_q ($q = 1, 2, c$ and m) is the transverse component of the wave vector in the x-direction, defined as

$$k_q = k_0\sqrt{n_q^2 - n_{\text{eff}}^2}. \tag{7}$$

Here, only the even mode will be considered as the interest is chiefly in the fundamental Bragg mode. Without loss of generality, the field amplitude at the core center is taken to be unity: $a_c^+ + a_c^- = 1$. Using the symmetry of the structure and the fact that the field inside the core should be real results in the relation $a_c^+ = a_c^- = 1/2$. The total field amplitudes inside the matching layer can be simply derived by applying the appropriate boundary condition of $\psi_j(x)$ continuity at $x = t_c/2$. The following expressions could be found for TE polarization:

$$\begin{aligned} a_m^+ &= \frac{1}{2}\cos\left(k_c\frac{t_c}{2}\right)e^{-ik_m t_m} \\ &\quad - i\frac{1}{2}\frac{k_c}{k_m}\sin\left(k_c\frac{t_c}{2}\right)e^{-ik_m t_m} \\ a_m^- &= \frac{1}{2}\cos\left(k_c\frac{t_c}{2}\right)e^{+ik_m t_m} \\ &\quad + i\frac{1}{2}\frac{k_c}{k_m}\sin\left(k_c\frac{t_c}{2}\right)e^{+ik_m t_m} \end{aligned} \tag{8}$$

while for TM polarization the following expression is obtained:

$$\begin{aligned} a_m^+ &= \frac{1}{2}\cos\left(k_c\frac{t_c}{2}\right)e^{-ik_m t_m} \\ &\quad + i\frac{1}{2}\frac{k_c}{k_m}\frac{n_m^2}{n_c^2}\sin\left(k_c\frac{t_c}{2}\right)e^{-ik_m t_m} \\ a_m^- &= \frac{1}{2}\cos\left(k_c\frac{t_c}{2}\right)e^{+ik_m t_m} \\ &\quad - i\frac{1}{2}\frac{k_c}{k_m}\frac{n_m^2}{n_c^2}\sin\left(k_c\frac{t_c}{2}\right)e^{+ik_m t_m}. \end{aligned} \tag{9}$$

The interface between the matching layer and the first unit cell of the Bragg stack at $x = \Delta_m$ is the entry point of the field into the periodic Bragg mirrors, where it is coupled into one of the supported Bragg modes. Using Bloch–Floquet formalism, the field amplitudes in the matching layer can be related to the elements of the unit cell translation matrix of TBRs, $A_{\text{TE(TM)}}$ and $B_{\text{TE(TM)}}$, according to [12]

$$\begin{aligned} a_m^+ &= B_{\text{TE(TM)}} \\ a_m^- &= e^{iK_{\text{TE(TM)}}\Lambda} - A_{\text{TE(TM)}}. \end{aligned} \tag{10}$$

For the QtW Bragg stack, the elements of the unit cell translation matrix for TE polarization are given as [12], [16]

$$\begin{aligned} A_{\text{TE}} &= -\frac{1}{2}\left(\frac{k_2}{k_1} + \frac{k_1}{k_2}\right) \\ B_{\text{TE}} &= +\frac{1}{2}\left(\frac{k_2}{k_1} - \frac{k_1}{k_2}\right) \\ e^{iK_{\text{TE}}\Lambda} &= -\left(\frac{k_2}{k_1}\right) \end{aligned} \tag{11}$$

and those for TM polarization are

$$\begin{aligned} A_{\text{TM}} &= -\frac{1}{2}\left(\frac{n_2^2 k_1}{n_1^2 k_2} + \frac{n_1^2 k_2}{n_2^2 k_1}\right) \\ B_{\text{TM}} &= +\frac{1}{2}\left(\frac{n_2^2 k_1}{n_1^2 k_2} - \frac{n_1^2 k_2}{n_2^2 k_1}\right) \\ e^{iK_{\text{TM}}\Lambda} &= -\left(\frac{n_1^2 k_2}{n_2^2 k_1}\right) \quad \left(n_1^2 k_2 < n_2^2 k_1\right) \end{aligned} \tag{12}$$

$$e^{iK_{\text{TM}}\Lambda} = -\left(\frac{n_2^2 k_1}{n_2^1 k_2}\right) \quad \left(n_1^2 k_2 > n_2^2 k_1\right). \tag{13}$$

In (11)–(13), $K_{\mathrm{TE(TM)}}$ is the Bloch wavenumber

$$K_{\mathrm{TE(TM)}} = \frac{1}{\Lambda}\arccos\left[Re\left(A_{\mathrm{TE(TM)}}\right)\right]. \tag{14}$$

Simple mode dispersion equations can be deduced with QtW-TBR. For TE-polarized wave, this can be obtained by adding the expressions in (8) and employing (10) to obtain

$$\tan(k_c t_c/2)\tan(k_m t_m) = \frac{k_m}{k_c}. \tag{15}$$

Similarly, for TM polarization, the equations in (9) can be subtracted for the case where $(n_1^2 k_2 < n_2^2 k_1)$ and added for the case where $(n_1^2 k_2 > n_2^2 k_1)$ to yield

$$\begin{aligned}\cot(k_c t_c/2)\tan(k_m t_m) &= -\frac{k_c}{k_m}\frac{n_m^2}{n_c^2} \quad \left(n_1^2 k_2 < n_2^2 k_1\right)\\ \tan(k_c t_c/2)\tan(k_m t_m) &= +\frac{k_m}{k_c}\frac{n_c^2}{n_m^2} \quad \left(n_1^2 k_2 > n_2^2 k_1\right).\end{aligned} \tag{16}$$

Given the mode index of QtW-BRW and material index x_m, the required matching layer thickness t_m can be easily obtained from (15) and (16). For TE polarization, it was found as

$$t_m = \frac{1}{k_m}\tan^{-1}\left[\frac{k_m}{k_c}\cot\left(k_c\frac{t_c}{2}\right) + p\pi\right] \tag{17}$$

where $p = 0, \pm 1, \pm 2, \ldots$, and for TM polarization it was

$$\begin{aligned} t_m &= \frac{1}{k_m}\tan^{-1}\left[-\frac{n_m^2}{n_c^2}\frac{k_c}{k_m}\tan\left(k_c\frac{t_c}{2}\right) + p\pi\right]\\ &\quad \left(n_1^2 k_2 < n_2^2 k_1\right)\\ t_m &= \frac{1}{k_m}\tan^{-1}\left[+\frac{n_c^2}{n_m^2}\frac{k_m}{k_c}\tan\left(k_c\frac{t_c}{2}\right) + p\pi\right]\\ &\quad \left(n_1^2 k_2 > n_2^2 k_1\right). \end{aligned} \tag{18}$$

The above expressions are the generic dispersion relations and design equations of the BRW-ML. The equations will be used next to compare the performance of BRW-ML to that of conventional BRWs using SHG as a case study.

IV. Enhancing the Nonlinear Interaction Using MLs

Now that the formalism and relations governing the Bragg guided-mode behavior have been elucidated, the improvements afforded by BRW-MLs will be investigated. The material system used is $Al_xGa_{1-x}As$. The material indexes of $Al_xGa_{1-x}As$ were derived using the Gehrsitz model at a given wavelength at temperature $T = 293\,^{\circ}\mathrm{K}$ [22]. The effective modal indexes of both the FH and SH were obtained using the methods reported in [23] and [24], respectively. In what follows, modal properties of both structures will be studied while the PM condition is maintained for SHG with an FH at 1550 nm. Core thickness t_c, nonlinear coupling efficiency η, GVM, and GVD will be investigated. In order to illustrate the improvements offered by BRW-ML over its conventional counterpart, an optimized QtW-BRW without matching layers will be used as a reference point for comparison.

This reference structure will be referred to as $\mathrm{BRW_{opt}}$ throughout the remainder of this paper. The design of $\mathrm{BRW_{opt}}$ focused on maximizing the nonlinear coupling efficiency while operating at the QtW point. Previous simulations indicated that the SH coupling efficiency is maximized by increasing the contrast between the Bragg reflectors bi-layers [16]. As such, this was the route we have undertaken to define $\mathrm{BRW_{opt}}$ with maximal nonlinear conversion efficiency. In order to avoid two-photon absorption (2PA) in the structure, however, the highest refractive index (lowest Al concentration) used in the structure was taken to be that of $Al_{0.20}Ga_{0.80}As$. This maintains the half bandgap of the layers in the structure above the photon energy of FH [1]. The highest Al concentration in the structure was selected as $Al_{0.80}Ga_{0.20}As$ to minimize the oxidation of the exposed sample areas. Furthermore, the bi-layers of the TBRs were arranged such that the core was sandwiched by the layer with higher refractive index. In Fig. 2, this required $n_m = n_2$ with $n_2 > n_1$. This was essential to excite fundamental even Bragg mode where the field amplitude peaked in the middle of the core. The choice of placing a low index layer on the sides of the core was also feasible. However, this configuration results in the excitation of the fundamental odd Bragg mode, where the field vanishes at the core center while it peaks, with opposite signs, at the core interface with the TBRs. In a QtW-BRW, since the FH also peaks at the core center, the later configuration would minimize the modal overlapp between the harmonics. Given these limitations in the Bragg stack materials and their arrangement, the choice of core thickness and Al concentration are dictated by the QtW condition. This further highlights the limitations of optimizing such structures while being governed by the range of refractive indexes offered by a given material system and while operating at the QtW point. The core was considered as the only tuneable parameter during optimization. For maximal conversion efficiency, the optimum core material was found to be $Al_{0.62}Ga_{0.35}As$. The complete parameter set of the structure is summarized in Table I.

TABLE I
Simulated Parameters of $\mathrm{BRW_{opt}}$

Parameter	Value
(x_c, x_1, x_2)	$(0.62, 0.20, 0.80)$
(n_c, n_1, n_2) at ω	$(3.0593, 3.2647, 2.9771)$
(n_c, n_1, n_2) at 2ω	$(3.2238, 3.5306, 3.1204)$
(t_c, t_1, t_2)	(392 nm, 11 nm, 341 nm)
n_{eff}	3.0684
η	53.42 m^-1
GVM	2.4644 ps/mm
GVD (FH)	1.0892 $\mathrm{fs}^2/\mu\mathrm{m}$
GVD (SH)	4.6449 $\mathrm{fs}^2/\mu\mathrm{m}$
Number of stacks bi–layers	10

The design algorithm of a BRW-ML takes its inputs as the modal effective index (n_{eff}), the thicknesses and refractive indexes of the core and cladding bi-layers, and the ML refractive index. The thickness of the ML is then calculated using (17) and (18). Using similar arguments as discussed earlier for the excitation of the fundamental even Bragg mode, it is assumed that $n_m > n_c$. Also, we take $n_1 < n_2$ in all designs, although the other case of $n_1 > n_2$ can also be investigated as an extra degree of freedom. Based on the discussion in Section II, the phase-matched structure is inspected for modes with effective indexes limited to $n_2^{(\omega)} < n_{\mathrm{eff}} < n_2^{(2\omega)}$ with stacks layers designed to be quarter-wave thick at the SH wavelength. To investigate the properties of BRW-ML systematically, the param-

eter space of x_m and x_c is scanned, while noting the waveguide salient characteristics. Using this approach, the properties of a range of BRW-ML structures which satisfy the PM condition were examined. The parameters of these structures that are pertinent to efficient PM will be discussed next. Initial simulations indicated that maximized overlap integral between the modes, hence maximized nonlinear conversion efficiency, could be achieved when (x_c, x_1, x_2) were chosen to have lower index of refraction in comparison to x_m. The effect of this choice is an improved confinement of the TIR mode at the FH in the core, as will be discussed below. The fact that the core thickness of BRW-MLs is a predetermined parameter demonstrates the flexibility this class of structures offers in comparison to conventional BRWs. This is particularly important for reducing the insertion loss associated with end-fire coupling in free-space optics settings. For the structures studied here, as will be discussed in the next section, a locally optimum core thickness of $t_c = 530$ nm was found for maximizing the nonlinear coupling efficiency. This choice of core thickness implies ≈35% increase compared with the core thickness of $\mathrm{BRW_{opt}}$. Also, in the design of the matching layers, (18) was used with $p = +1$. This provided significant enhancements in the parameters of interest for SHG when compared to those obtained for $p = 0$. The range of values spanned for x_m and x_c is $0.35 < x_m < 0.40$ and $0.55 < x_c < 0.75$. This ensured that there exist Bragg modes where the PM condition could be satisfied, while the other layers adhere to the restrictions on the Al content discussed earlier. The TBRs consist of $Al_{0.40}Ga_{0.60}As$–$Al_{0.80}Ga_{0.20}As$ bi-layers ($x_1 = 0.80$, $x_2 = 0.40$) with ten periods to provide stack reflectivity close to unity.

A. Nonlinear Coupling Efficiency

Nonlinear coupling efficiency η is a key parameter in determining the conversion efficiency in a SHG process. In a nonlinear multilayer waveguide with length L, η is defined as

$$\eta = \frac{I^{(2\omega)}}{\left(I^{(\omega)}\right)^2} = 2\left(\frac{\mu_0}{\epsilon_0}\right)^{\frac{3}{2}} \frac{\omega^2 L^2 d_m^2}{n_{\mathrm{eff}}^3 t_{\mathrm{SHG}}^{\mathrm{eff}}} \tag{19}$$

where $I^{(\omega)}$ and $I^{(2\omega)}$ are the field intensities of FH and SH, respectively, d_m is the maximum effective SH coefficient and $t_{\mathrm{SHG}}^{\mathrm{eff}}$ is the effective thickness for SHG. It is defined as

$$t_{\mathrm{SHG}}^{\mathrm{eff}} = \frac{\left[\int_{-\infty}^{\infty} d'(x)\left[E_x^{(2\omega)}(x)\right]\left[E_y^{(\omega)}(x)\right]^2 dx\right]^2}{\left[\int_{-\infty}^{\infty}\left[E_y^{(\omega)}(x)\right]^2 dx\right]^2 \left[\int_{-\infty}^{\infty}\left[E_x^{(2\omega)}(x)\right]^2 dx\right]}. \tag{20}$$

The term $d'(x) = d(x)/d_{\max}$ is the normalized SH coefficient. Enhancement of η, can be primarily achieved by increasing, L, as well as decreasing $t_{\mathrm{SHG}}^{\mathrm{eff}}$. Although theoretically the waveguide length is a more effective parameter due to its quadratic relation with η, in practice this is not the case when linear and nonlinear propagation losses are taken into account. On the other hand, optimal waveguide designs can enhance the growth of η by means of reducing $t_{\mathrm{SHG}}^{\mathrm{eff}}$. The flexibility offered by BRW-MLs help achieving this goal. In Fig. 3, the contour plot of normalized coupling efficiency, $n_{\mathrm{eff}}^{-3}/t_{\mathrm{SHG}}^{\mathrm{eff}}$, as a function of (x_c, x_m) is shown. Noticeable improvement is readily achieved for larger x_c with smaller x_m. For $(x_c, x_m) = (0.71, 0.35)$, η increases from $\approx 53.4\ \mathrm{m^{-1}}$ for $\mathrm{BRW_{opt}}$ to $\approx 840\ \mathrm{m^{-1}}$ for this optimized BRW-ML structure. This improvement by over an order of magnitude offers substantial advantages for many applications where nonlinear conversion efficiency is important, including optical parametric oscillators and photon-pair sources. In order to better understand how the matching layer affects the nonlinear coupling efficiency, the normalized fields of the two designs were plotted as illustrated in Fig. 4. The enhanced η in BRW-ML can be attributed to three factors. First, the inclusion of the matching layer assists in increasing the core dimension, where the overlap between the harmonics is maximum. Second, within the first period of the Bragg stacks where the fields of the harmonics are at opposite phases in $\mathrm{BRW_{opt}}$, BRW-ML benefits from weaker out of phase field

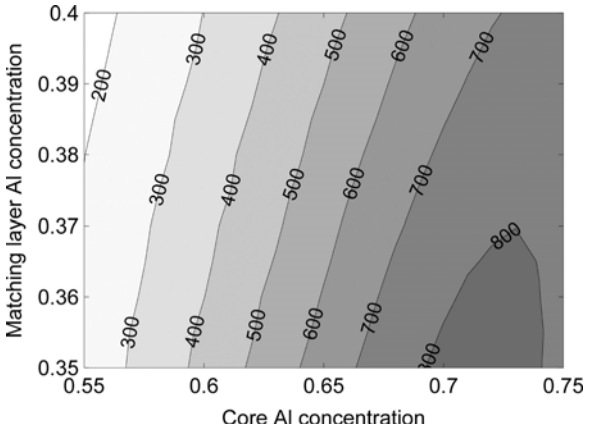

Fig. 3. Nonlinear coupling efficiency, η [$\mathrm{m^{-1}}$], as a function of (x_c, x_m) for BRW-ML, with $(x_1, t_1) = (0.80, 492\ \mathrm{nm})$, $(x_2, t_2) = (0.40, 147\ \mathrm{nm})$ and $(t_c, t_m) = (530\ \mathrm{nm}, 435\ \mathrm{nm})$. A maximum nonlinear coupling efficiency of $\approx 840\ \mathrm{m^{-1}}$ is obtained at $(x_c, x_m) = (0.71, 0.35)$.

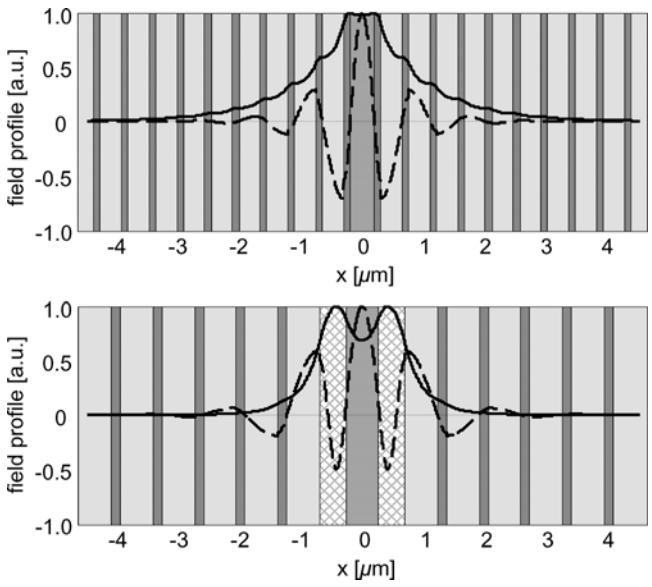

Fig. 4. Normalized profiles of (a) $\mathrm{BRW_{opt}}$ and (b) BRW-ML with $(x_c, x_m) = (0.71, 0.35)$ and with other parameters given in Fig. 3. In both figures, the solid line is $E_y^{(\omega)}(x)$ for TE-polarized FH, and the dashed line is $E_x^{(2\omega)}(x)$ for TM-polarized SH.

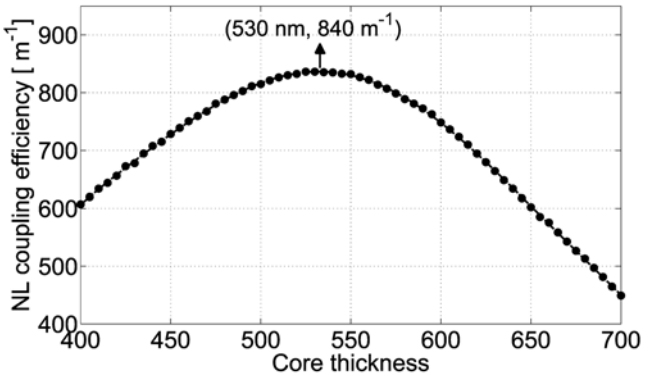

Fig. 5. Nonlinear coupling efficiency, η [m^{-1}], as a function of core thickness with $(x_c, x_m) = (0.71, 0.35)$. Other parameters are identical to those given in Fig. 3. Maximum nonlinear coupling of 840 m^{-1} is obtained at $t_c = 530$ nm, which is attributed to the enhanced overlap of the fields profile offered by BRW-ML.

amplitudes. Third, the inclusion of the ML results in the sign change of the SH field within the n_2 layer beside the ML which gives rise to constructive overlap between the profiles. A useful figure of merit which represents the ML control over the field profiles of the harmonics is the confinement factor, Γ. It is defined as the ratio between the power within the core to the overall mode power. It should be noted that in obtaining Γ for BRW-ML, depending on the effective mode index at PM point, the actual core might be regarded as the original core layer, n_c, or as a three-layer core composed of the original core with the MLs. Taking this into consideration, for the FH, Γ was found to be $\approx$0.31% for $\mathrm{BRW_{opt}}$ and increased to $\approx$0.86% for the BRW-ML with $(x_c, x_m) = (0.71, 0.35)$, where maximum η was obtained. For the same structures, the enhancement in Γ was less pronounced for the SH. In this case, the confinement factor was increased from $\approx$0.43% for $\mathrm{BRW_{opt}}$ to $\approx$0.67% for BRW-ML. Also, it would be instructive to compare the propagation loss of the two designs. Using the method proposed in [24] the loss at 2ω was obtained to be $\approx$7.6 dB/cm for $\mathrm{BRW_{opt}}$ and $\approx 7.3 \times 10^{-2}$ dB/cm for BRW-ML with $(x_c, x_m) = (0.71, 0.35)$. This noticeable reduction in the SH loss, by approximately two orders of magnitude, can theoretically enhance the nonlinear conversion efficiency. However, in practice, one can expect to experience higher loss values due to material absorption, TPA, as well as scattering by rough etched surfaces and interfaces.

To further investigate the effect of t_c on the nonlinear coupling factor, the dependence of η on the core thickness is illustrated in Fig. 5. From the figure, the peak nonlinear coupling of 840 m^{-1} occurs at $t_c = 530$ nm which justifies the choice of the core thickness. The existence of an optimum (η, t_c) pair can also be important from a practical perspective. Due to strong dependence of modal dispersion properties on core thickness in BRWs, operating at the optimum t_c results in reducing the sensitivity of the design to unavoidable fabrication tolerances during growth. Notice that the design of $(x_c, x_m, t_c) = (0.71, 0.35, 530\,\mathrm{nm})$ is not necessarily a global optimum, it is a representative design with substantial advantages over its conventional BRW counterpart. A global optimum might be attained through advanced nonlinear optimization algorithms.

An important factor in the operation of phase-matched BRWs is whether the structure supports multimode propagation at FH wavelength. Ideally, it is desired to design the phase-matched structure to be single moded where the PM condition is satisfied only between the fundamental even TIR and BRW modes at the design wavelength. This ensures maximum interaction and hence conversion efficiency between the interacting waves. It is practically challenging to avoid exciting higher order modes if they exist. For $\mathrm{BRW_{opt}}$, it was verified that the structure was supporting only the fundamental TIR and BRW modes. However, for all the structures in Fig. 5, the lowest order odd mode was also guided. This mode has much lower coupling efficiency from objective lenses used in end-fire coupling arrangements. It also has much lower overlap and, hence, conversion efficiency with the fundamental BRW mode.

B. GVM and GVD

In parametric processes involving ultrashort pulses, temporal pulse walk-off between the harmonics substantially degrades the nonlinear conversion efficiency. The two signals which initially overlap in time lose this overlap due to the mismatch between their group velocities. Quantitatively, this can be expressed by the GVM between the harmonics, which is defined as

$$\mathrm{GVM} = \left| \frac{1}{v_g^{(\omega)}} - \frac{1}{v_g^{(2\omega)}} \right| = \frac{1}{c} \left| n_g^{(\omega)} - n_g^{(2\omega)} \right| \qquad (21)$$

where $n_g^{(\omega)}$ and $n_g^{(2\omega)}$ are the group indexes at ω and 2ω, respectively. The effect of GVM becomes particularly pronounced in parametric processes, where some of the interacting harmonics are in proximity to the waveguide material bandgap. However, the control of waveguide dispersion offered by BRWs serves to mitigate the effect of GVM on reducing the effective interaction length. The contour plot of group velocity mismatch for BRW-ML is illustrated in Fig. 6. From the figure, a minimum GVM of $\approx$1.73 ps/mm was obtained for $(x_c, x_m) = (0.75, 0.35)$. In comparison with $\mathrm{BRW_{opt}}$, the new structure benefits from $\approx$30% reduction in GVM. This reduction is associated with a corresponding increase in the effective interaction length of a waveguide utilizing the second-order nonlinearities using ultrashort pulses. For example, a picosecond pulse with typical pulse bandwidth (FWHM) of 4 pm, using $\mathrm{BRW_{opt}}$, the useful interaction length is limited to $\approx$1.6 mm before significant temporal walk-off between the harmonics, while the device length is increased to $\approx$2.3 mm by using the BRW-ML design with $(x_c, x_m) = (0.75, 0.35)$. Tailoring the GVD is essential in many applications involving ultrashort pulses. Certain waveguide designs demand minimized GVD at the operating wavelength to reduce the pulse distortion along the propagation distance. In applications concerned with temporal solitons in materials with nonlinear refractive indices, GVD determines the threshold intensity for soliton formation [18]. In quantum optics, tailoring the GVD plays an important role in controlling the entanglement of photon pairs generated through spontaneous parametric down conversion (SPDC) [19]. Dispersion properties of QtW-BRWs have been comprehensively analyzed

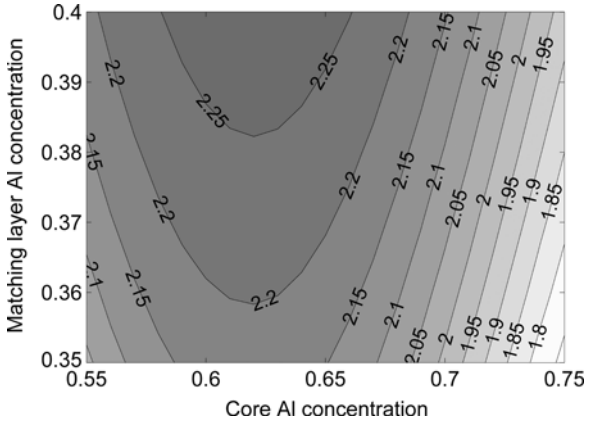

Fig. 6. GVM [ps/mm] between the harmonics as a function of (x_c, x_m) for BRW-ML. Minimum GVM of $\approx$ 1.73 ps/mm is obtained at $(x_c, x_m) = (0.75, 0.35)$ with $(t_c, t_m) = (530\text{ nm}, 373\text{ nm})$, $(x_1, t_1) = (0.80, 526\text{ nm})$, and $(x_2, t_2) = (0.40, 147\text{ nm})$.

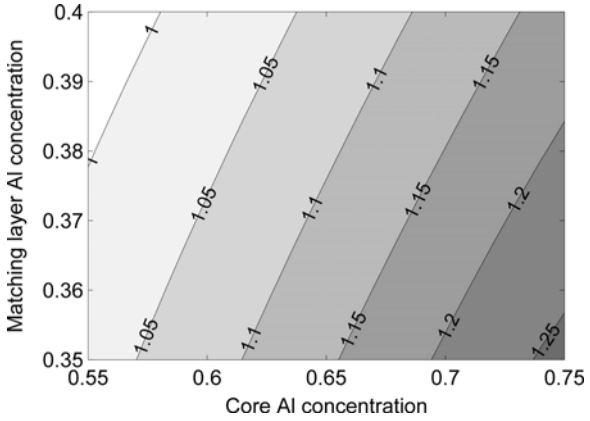

Fig. 7. GVD [fs$^2/\mu$m] of BRW-ML at ω. Minimum GVD of 0.98 fs$^2/\mu$m is modelled at $(x_c, x_m) = (0.55, 0.40)$ with $(t_c, t_m) = (530\text{ nm}, 373\text{ nm})$, $(x_1, t_1) = (0.80, 530\text{ nm})$ and $(x_2, t_2) = (0.40, 147\text{ nm})$.

in [20] using perturbation method. Here, we present the numerical modelling of GVD for phase-matched BRW-ML. By definition

$$\text{GVD} = \frac{\partial^2 \beta}{\partial \omega^2} = \frac{2}{c}\frac{\partial n_{\text{eff}}}{\partial \omega} + \frac{\omega}{c}\frac{\partial^2 n_{\text{eff}}}{\partial \omega^2}. \tag{22}$$

Plots of GVD versus (x_c, x_m) for FH and SH are shown in Figs. 7 and 8, respectively. At ω, GVD decreases with the increase of x_m. For the choice of (x_c, x_m), where nonlinear coupling efficiency is high, the GVD of the FH is larger compared with that of the BRW_{opt}. However, using BRW-ML affords designs with reduced GVD. One examples is obtained for $(x_c, x_m) = (0.55, 0.40)$, where the group velocity dispersion drops to ≈ 0.98 fs$^2/\mu$m. This translates to a reduction of $\approx$10%. The GVD at 2ω exhibits stronger variations with respect to the design parameters. A minimum GVD of ≈ 2.21 fs$^2/\mu$m is obtained for $(x_c, x_m) = (0.75, 0.40)$. In the picosecond regime, the effect of GVD on SH pulses is negligible and becomes severe when optical pulses as short as a few tens of femtoseconds are employed [26], [27]. To overcome the problem of pulse distortion, usually the interaction length of the device is reduced at the expense of NL interaction efficiency. The capability of BRW-MLs to provide reduced GVD at the SH can offer significant advantages for SHG with ultrashort pulses without sacrificing the effective interaction length. It should be noted that the parameter space, namely (x_c, x_m), where GVD is small at the SH partly overlaps with that providing large nonlinear coupling coefficient. The capability of enhancing the effective nonlinearity while reducing the GVD has not been previously possible in other PM schemes to the best of our knowledge.

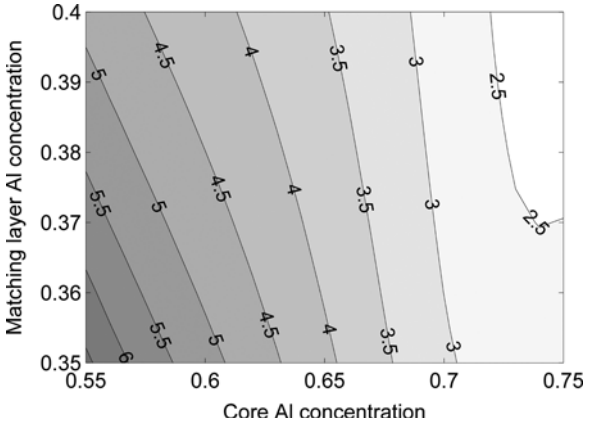

Fig. 8. GVD [fs$^2/\mu$m] of BRW-ML at 2ω. Minimum GVD of 2.21 fs$^2/\mu$m is modelled at $(x_c, x_m) = (0.75, 0.40)$ with $(t_c, t_m) = (530\text{ nm}, 457\text{ nm})$, $(x_1, t_1) = (0.80, 392\text{ nm})$ and $(x_2, t_2) = (0.40, 143\text{ nm})$.

V. Conclusion

A general procedure for the design of PM BRW-ML was presented. Using Bloch–Floquet formalism, dispersion equations of both TE and TM modes were derived for these structures. Nonlinear coupling efficiency was shown to benefit the most from the BRW-ML, due to the enhanced overlap factor of the interacting harmonics. GVM and the GVD of the FH could be reduced by using the matching layer approach in comparison to conventional BRWs. In addition, BRW-ML enables additional control over tailoring the GVD of both FH and SH. The attractive features demonstrated for using BRW-ML to facilitate PM makes it an optimal approach for frequency conversion via second order nonlinearities in semiconductors. This control over the phase matching properties is attractive for more advanced applications such as those utilizing quantum optical effects and parametric oscillators.

References

[1] A. S. Helmy, D. C. Hutchings, T. C. Kleckner, J. H. Marsh, A. C. Bryce, J. M. Arnold, C. R. Stanley, J. S. Aitchison, C. T. A. Brown, K. Moutzouris, and M. Ebrahimzadeh, "Quasi phase matching in GaAs–AlAs superlattice waveguides via bandgap tuning using quantum well intermixing," *Opt. Lett.*, vol. 25, no. 18, pp. 1370–1372, Sep. 2000.

[2] A. Fiore, S. Janz, L. Delobel, P. van der Meer, P. Bravetti, V. Berger, and E. Rosencher, "Second-harmonic generation at $\lambda = 1.6$ μm in AlGaAs/Al_2O_3 waveguides using birefringence phase matching," *Appl. Phys. Lett.*, vol. 72, pp. 2942–2945, Jun. 1998.

[3] R. Haidar, N. Forget, and E. Rosencher, "Optical parametric oscillation in micro-cavities based on isotropic semiconductors: A theoretical study," *IEEE J. Quantum Electron*, vol. 39, no. 4, pp. 569–576, Apr. 2003.

[4] A. S. Helmy, "Phase matching using Bragg reflection waveguides for monolithic nonlinear optics applications," *Opt. Exp.*, vol. 14, no. 3, pp. 1243–1252, Feb. 2006.
[5] B. R. West and A. S. Helmy, "Analysis and design equations for phase matching using Bragg reflection waveguides," *IEEE J. Sel. Top. Quantum Electron.*, vol. 12, no. 3, pp. 431–442, May–Jun. 2006.
[6] R. Das and K. Thyagarajan, "SHG in Bragg reflection waveguides for enhanced bandwidth applications," *J. Opt. Commun.*, vol. 270, no. 1, pp. 79–84, Feb. 2007.
[7] A. S. Helmy, B. Bijlani, and P. Abolghasem, "Phase matching in monolithic Bragg reflection waveguides," *Opt. Lett.*, vol. 32, no. 16, pp. 2399–2401, Aug. 2007.
[8] B. Bijlani, P. Abolghasem, and A. S. Helmy, "Second harmonic generation in ridge Bragg reflection waveguides," *Appl. Phys. Lett.*, vol. 92, pp. 1011241–1011243, 2007.
[9] A. Mizrahi and L. Schächter, "Bragg reflection waveguides with a matching layer," *Opt. Exp.*, vol. 12, no. 14, pp. 3156–3170, Jul. 2004.
[10] A. Mizrahi and L. Schächter, "Optical Bragg accelerators," *Phys. Rev. E*, vol. 70, no. 016505, Jul. 2004.
[11] Y. Sakurai and F. Koyama, "Control of group delay and chromatic dispersion in tuneable hollow waveguide with highly reflective mirrors," *Jap. J. App. Phys.*, vol. 43, no. 8B, pp. 5828–5831, Aug. 2004.
[12] P. Yeh and A. Yariv, "Bragg reflection waveguides," *Opt. Commun.*, vol. 19, no. 3, pp. 427–430, Dec. 1976.
[13] S. R. A. Dods, "Bragg reflection waveguide," *J. Opt. Soc. Am. A.*, vol. 6, no. 9, pp. 1465–1476, Sep. 1989.
[14] D. B. Burckel and S. J. Brueck, "Generalized transverse Bragg waveguides," *Opt. Exp.*, vol. 13, no. 23, pp. 9202–9210, Nov. 2005.
[15] A. Yariv and P. Yeh, *Optical Waves in Layered Media*. New York: Wiley, 1988.
[16] B. R. West and A. S. Helmy, "Properties of the quarter-wave Bragg reflection waveguide: Theory," *J. Opt. Soc. Amer. B.*, vol. 23, no. 6, pp. 1207–1220, Jun. 2006.
[17] W. Liang, West, Y. Xu, J. M. Choi, and A. Yariv, "Engineering transverse Bragg resonance waveguides for large modal volume lasers," *Opt. Lett.*, vol. 28, no. 21, pp. 2079–2081, Nov. 2003.
[18] G. P. Agrawal, *Nonlinear Fiber Optics*. New York: Academic, 1989.
[19] R. Erdmann, D. Branning, W. Grice, and R. A. Walmsley, "Restoring dispersion cancellation for entangled photons produced by ultrashort pulses," *Phys. Rev. A.*, vol. 62, no. 5, p. 053810, Oct. 2000.
[20] B. R. West and A. S. Helmy, "Dispersion tailoring of the quarter-wave Bragg reflection waveguide," *Opt. Exp.*, vol. 14, no. 9, pp. 4073–4086, Apr. 2006.
[21] S. Wagner, A. Al Mehairy, J. S. Aitchison, and A. S. Helmy, "Modelling and optimization of qausi-phase matching using domain disordering," *IEEE J. Quantum Electron.*, vol. 44, no. 5, pp. 424–429, May 2008.
[22] S. Gehrsitz, F. K. Reinhart, C. Gourgon, N. Herres, A. Vonlanthen, and H. Sigg, "The refractive index of $Al_xG_{1-x}As$ below the bandgap: Accurate determination and empirical modeling," *J. Appl. Phys.*, vol. 87, no. 11, pp. 7825–7837, Jun. 2000.
[23] J. Chilwell and I. Hodgkinson, "Thin-films field-transfer matrix theory of planar multilayer waveguides and reflection from prism-loaded waveguides," *J. Opt. Soc. Amer. A*, vol. 1, no. 7, pp. 742–753, Jul. 1984.
[24] A. K. Ghatak, K. Thyagarajan, and M. R. Shenoy, "Numerical analysis of planar optical waveguides using matrix method," *J. Lightw. Technol.*, vol. LT-5, no. 5, pp. 660–667, May 1987.
[25] M. M. Fejer, G. A. Magel, D. H. Jundt, and R. L. Byer, "Quasi-phase-matched second harmonic generation: Tuning and tolerances," *IEEE J. Quantum Electron*, vol. 28, no. 11, pp. 2631–2654, Nov. 1992.
[26] E. Sidick, A. Knoesen, and A. Dienes, "Ultrashort-pulse second-harmonic generation. I. Transform-limited fundamental pulses," *J. Opt. Soc. Amer. B*, vol. 12, no. 9, pp. 1704–1712, Sep. 1995.
[27] E. Sidick, A. Knoesen, and A. Dienes, "Ultrashort-pulse second-harmonic generation. II. Non-transform-limited fundamental pulses," *J. Opt. Soc. Amer. B*, vol. 12, no. 9, pp. 1713–1722, Sep. 1995.

Payam Abolghasem received the B.A.Sc. degree in electrical engineering from the University of Ottawa, Ottawa, ON, Canada, in 2004 and the M.A.Sc. from McMaster University, Hamilton, ON, Canada, in 2006. He is currently working toward the Ph.D. degree at the University of Toronto, Toronto, ON.

His research interests are in nonlinear optical properties in III-V semiconductor materials, integrated optical parametric devices, semiconductor diode lasers, and computational electromagnetics.

Amr S. Helmy (M'99–SM'06) received the B.Sc. degree in electronics and telecommunications engineering from Cairo University, Cairo, Egypt, in 1993, and the M.Sc. and Ph.D. degrees with a focus on photonic fabrication technologies from the University of Glasgow, Glasgow, U.K., in 1994 and 1999, respectively.

Prior to his academic career, he held a position with Agilent Technologies Photonic Devices, R&D Division, in the U.K. At Agilent, his responsibilities included developing distributed-feedback lasers, monolithically integrated lasers, modulators, and amplifiers in InP-based semiconductors. He also developed high-powered submarine-class 980-nm InGaAs pump lasers. He is currently an Assistant Professor with the Edward S. Rogers Sr. Department of Electrical and Computer Engineering, University of Toronto, Toronto, ON, Canada. His research interests include photonic device physics and characterization techniques (with an emphasis on nonlinear optics in III-V semiconductors), applied optical spectroscopy in III-V optoelectronic devices and materials, and III-V fabrication and monolithic integration techniques.

Dr. Helmy is a member of the Optical Society of America.